nanomaterials

MDPI

Article

Investigations of 2D PtS_2's Saturable Absorption Characteristic and Its Optimization to OPO's Operation

Xinyu Hu, Jing Wang *, Heze Guo, Kai Jiang, Wenjing Tang * and Wei Xia

School of Physics and Technology, University of Jinan, Jinan 250022, China; hxy2237623598@163.com (X.H.); ghz772767365@163.com (H.G.); sps_jiangk@ujn.edu.cn (K.J.); sps_xiaw@ujn.edu.cn (W.X.)
* Correspondence: ss_wangj@ujn.edu.cn (J.W.); sps_tangwj@ujn.edu.cn (W.T.)

Abstract: A 6.2 nm-thickness platinum disulfide (PtS_2) film was prepared by electron beam evaporation with post vulcanization. The nonlinear transmittance was measured by power scanning method and the modulation depth is fitted to be 13%. Based on the transmittance curve, saturable absorption parameters of PtS_2 are calculated with inhomogeneously broadening mechanism, including 6.4298 $\times$ 10^{-19} cm^{-2} ground-state absorption cross-section, 2.5927 $\times$ 10^{-19} cm^{-2} excited-state absorption cross-section, and 1.043 ms excited-state lifetime. The PtS_2 film combined with active time management was implemented to modulate the fundamental light of optical parametric oscillator (OPO). Owing to the nonlinear absorption property of PtS_2, the operation of Q-switched OPO was optimized in both the experiment and dynamical theory. In particular, the conversion efficiency was experimentally improved by 13.2%. The pump-to-signal conversion efficiency went up to 3.29%, which is the highest conversion value reported so far. The theoretical values fit the experiment well, which are from the Gaussian rate equations with PtS_2's saturable-absorption characteristic.

Keywords: nanotechnology; 2D PtS_2; saturable absorption; nonlinear frequency conversion; optical parametric oscillator

Citation: Hu, X.; Wang, J.; Guo, H.; Jiang, K.; Tang, W.; Xia, W. Investigations of 2D PtS_2's Saturable Absorption Characteristic and Its Optimization to OPO's Operation. *Nanomaterials* **2022**, *12*, 1670. https://doi.org/10.3390/nano12101670

Received: 22 April 2022
Accepted: 11 May 2022
Published: 13 May 2022

1. Introduction

As passive modulators for laser pulses, two-dimensional (2D) transition metal sulfides (TMDCs) have attracted much attention in recent years, because of the advantages of fast recovery time, high modulation depth, and low preparing cost [1,2]. As a member of the TMDCs family, the few-layer platinum disulfide (PtS_2) consists of S–Pt–S atoms in the plane, and there are strong covalent bonding and weak van der Waals bonding between the layers [3,4]. Few-layer PtS_2 is promising in 1μm-and-above-wavelength laser modulation, and its bandgap ranges from 0.25 eV for bulk to 1.6 eV for monolayer [5–9]. At present, 2D PtS_2 has been applied to fiber laser to obtain 1 μm or 1.5 μm-wavelength pulse [5,10,11]. Although 2D TMDC has been proven to have a high damage threshold and a high switching ratio, layered PtS_2 has not been reported to be used in solid-state lasers as a passive modulator [12–15].

Based on second-order nonlinear frequency conversion, optical parametric oscillator (OPO) can generate 1.5–1.6 μm coherent eye-safe light [16,17]. Compared to extracavity OPO, the high photon density of fundamental laser for the intracavity OPO (IOPO) can be fully utilized to generate signal or idler pulses with high single-pulse energy. For a Q-switched IOPO, the shorter width and higher peak fundamental laser contribute to higher conversion [18,19]. Although the lasers Q-switched by 2D TMDCs are reported a lot, few of them have been applied to OPO's fundamental lasers because of the low time-stability of pulse sequence [20–23]. If an active Q-switch is introduced to manage the action time of the saturable absorber (SA), the IOPO modulated by 2D PtS_2 is prospected. Moreover, due to PtS_2's saturable absorption characteristic, the experimental optimization of Q-switched IOPO could be realized.

Dynamic rate equations are effective in guiding the experiments of lasers or OPOs based on PtS_2 [24,25]. Compared with the plane-wave approximation results, the theoretical calculations are better fitted to the experimental results when considering the Gaussian spatial distribution of the fundamental photon [26,27]. So far, few works have been involved in the Gaussian rate equations of IOPOs. The saturation absorption parameters of PtS_2 are needed to solve the dynamic equations, and they are also the keys to obtaining narrow-pulse and high peak-power lasers. As the energy band structure of PtS_2 is still being researched, the values of SA parameters are rarely reported, including the ground-state absorption cross-section, the excited-state absorption cross-section, and the excited-state lifetime. Therefore, a dynamical investigation of lasers modulated by PtS_2 has not been reported in the literature, especially not an IOPO pumped by it.

In this work, a few-layer PtS_2 SA was prepared by the method of electron beam evaporation (EBE) method, and its optical properties were thoroughly investigated. Considering the inhomogeneously broadening mechanism, the SA parameters of PtS_2 were estimated from the measured transmittance curves. Then, the dynamic coupling rate equations under the Gaussian spatial distribution were derived and solved for a Q-switched IOPO with PtS_2. Finally, in our experiment, a signal-resonant KTP IOPO based on the prepared PtS_2 SA was realized. The acousto-optic (AO), as an active modulator, was used to control the fundamental-pulse-repetition rate. The few-layer PtS_2 SA was used to optimize the performance of Q-switched IOPO as a passive Q-switch. The optimization of PtS_2 SA to IOPO was analyzed, including the pulse-width compression, the peak-power improvement, the pulse-sequence stability and the nonlinear-conversion-efficiency promotion. The theoretical results are in reasonable agreement with the experimental values.

2. Material Fabrication and Characterization in Experiment

PtS_2 thin film was synthesized by metal film plus post-sulfurization treatment [28]. In the first step, the Pt film was deposited on c-cut sapphire (Al_2O_3 substrate) by using an electron beam evaporation furnace (ATS 500, HHV, West Sussex, UK). After that, the Pt-coated Al_2O_3 substrate was thermally annealed in a sulfur-rich ambiance for 30 min. During the thermal treatment, a flow of 80 sccm H_2S was introduced for sulfurization and the Ar/H_2 mixture of 225 sccm/75 sccm was employed as a carrier gas and reactive gas. Finally, the PtS_2 sample was removed for characterization. The PtS_2 SA is characteristically summarized in Figure 1. The Raman spectrum of the PtS_2 SA was measured by a Raman spectrometer (Horiba LabRAM HR Evolution, Kyoto, Japan), excited by a 532 nm laser. As shown in Figure 1a, the two characteristic peaks at 260 cm^{-1} and 336 cm^{-1} correspond to the in-plane E^1_{2g} vibrational mode and the out-of-plane A_{1g} vibrational mode, respectively. The frequency interval between the two peaks is 76 cm^{-1}. As has already been established, the E^1_{2g} mode is related to the in-plane vibration of the S and Pt atoms heading in opposite directions. The A_{1g} mode is related to the out-of-plane motion of the S atom, which reflects the coupling between layers. The A_{1g} peak of PtS_2 prepared in this experiment is blue-shifted by 2 cm^{-1} compared with bulk-like PtS_2, which implies the 2D nanostructure [12,14]. The optical micrograph (CX23, Olympus, Tokyo, Japan) measured in Figure 1b demonstrates the contrast between the PtS_2 sample and pristine transparent sapphire substrate. The color contrast of the sample indicates that the sample is a few-layer film. Figure 1c shows the atomic force microscopy (AFM, Bruker Dimension Icon, Billerica, MA, USA) where the thickness and the corresponding height diagram are given. As illustrated in the figure, the thickness of PtS_2 is approximately 6.2 nm. Considering the 5.03 Å thickness of single-layer and 3.07 Å interplanar spacing for PtS_2 [29,30], the structure of the sample is approximately 8 layers, which corresponds to the abovementioned optical micrograph and Raman spectrum analysis results.

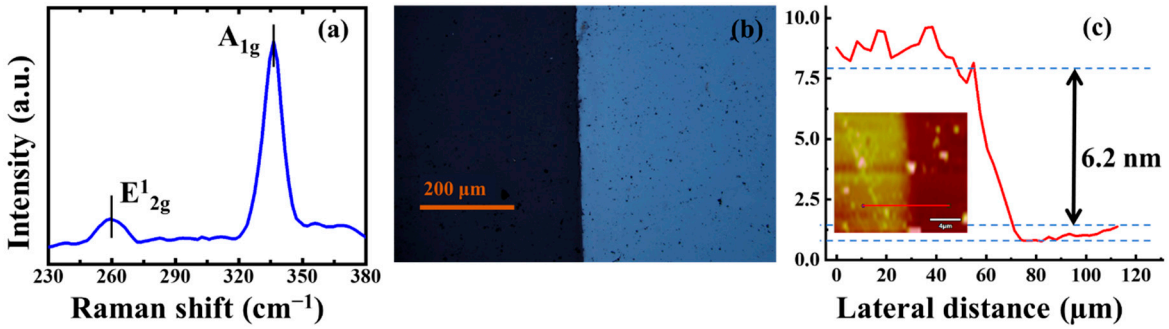

Figure 1. Characteristic of the prepared PtS_2. (**a**) Optical micrograph; (**b**) Raman spectrum; (**c**) Atomic force microscopy.

The nonlinear transmittance of PtS_2 SA versus different incident peak power intensity is measured by double-optical-path method [31]. An AO Q-switched solid-state laser (1.06 μm wavelength, 120 ns pulse width, 15 kHz repetition rate) was used as the laser source. The nonlinear transmittance of the sample is shown in Figure 2a. The approximated nonsaturable loss (α_s), initial transmittance (T_0), and saturation transient intensity (I_{sat}) were fitted as 9.3%, 77.0%, and 1.077 MW/cm^2, respectively, and then the modulation depth (ΔT) was calculated to be 13%. With the increasing peak-energy density at the low power density, the material transmittance increases linearly, as shown in Figure 2b. The slope obtained by linear fitting is 1.14.

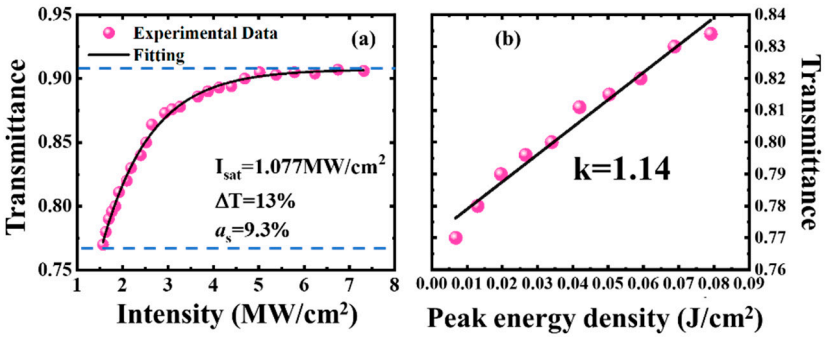

Figure 2. Optical characteristics of PtS_2. (**a**) The transmittance of PtS_2 SA versus incident power intensity. (**b**) The linear relation for low-power density.

3. Theoretical Evaluation of IOPO with 6.2 nm-Thick PtS_2's Saturable Absorption Characteristic

In theory, Q-switching dynamics is well explained by rate equations [32]. In this section, the Gaussian assumption and PtS_2's characteristic were considered for the dynamical model of a Q-switched Nd:YVO_4/KTP IOPO with AO active time-management.

3.1. Gaussian Rate Equations of IOPO

The Gaussian transversal distribution and longitudinal distribution of the photon density in the cavity are considered in the rate equations, as well as the thermal effect of the gain medium. The average intracavity photon density $\phi(r,t)$ of the TEM_{00} mode can be represented by

$$\phi(r,t) = \phi(0,t)\exp\left(-\frac{2r^2}{w_l^2}\right) \quad (1)$$

In this formula, w_l is the average beam radius of the fundamental light.

$$\phi_j(r,t) = \frac{w_l^2}{w_j^2}\phi_j(0,t)\exp\left(-\frac{2r^2}{w_j^2}\right)(j = g,a,y,p,s,i) \quad (2)$$

where $\phi_j(0,t)(j = s, i)$ represents the intracavity photon densities of the signal light and idler light; $\phi_j(0,t)(j = g, a, y)$ represents the fundamental light intracavity photon densities at the positions of Nd: YVO_4 crystal, AO crystal, and PtS_2 SA, respectively [33]; w_j ($j = g$, a, y) represents the radius of the TEM_{00} mode in the abovementioned three positions. The relationship between the photon densities and the electric field is represented by $\phi(r,t) = \varepsilon E^2(r,t)/4h\omega$. Considering the transverse Gaussian distribution of beam energy, $E_j(r,t) = E_j(0,t)\exp(-r^2/w_j^2)$ can be derived, where $E(r,t)$ is the electrical field. $E_j(0,t)$ ($j = p$, s, i) is the electrical field of the fundamental light, the signal light and the idler light on the laser axis.

Under Gaussian assumption, the excited-state population densities $n_{y1}(r,t)$ of the saturable absorber can be expressed as

$$n_{y1}(r,t) = n_{y1}(0,t)\exp\left(-\frac{2r^2}{w_y^2}\right) \tag{3}$$

The IOPO rate equation with the saturable absorption characteristic of PtS_2 SA is obtained by referring to the previous research work [26,27,32,33].

$$\begin{aligned}&\int_0^\infty \tfrac{d\phi(r,t)}{dt}\cdot 2\pi r dr = \\ &\int_0^\infty \tfrac{1}{t_r}\cdot\left[2\sigma l_g n(r,t)\phi_g(r,t) - (\sigma_g - \sigma_e) l_y n_{y1}(r,t)\phi_y(r,t) - \sigma_e l_y n_{y0}\phi_y(r,t)\right] \\ &\cdot 2\pi r dr - \int_0^\infty \tfrac{1}{t_r}\cdot\left[\delta_T(t)\phi_g(r,t) + \delta_a(t)\phi_a(r,t)\right]\cdot 2\pi r dr - \int_0^\infty \tfrac{\delta I w_k^2}{8h w_l^2}\cdot\tfrac{l_{opo}}{l}\cdot\tfrac{l_{KTP}}{l_{opo}} \\ &\cdot E_p(r,t)E_s(r,t)E_i(r,t)\cdot 2\pi r dr\end{aligned} \tag{4}$$

$$\int_0^\infty \frac{d\phi_s(r,t)}{dt}\cdot 2\pi r dr = \int_0^\infty \left[-\frac{\phi_s(r,t)}{\tau_s} + \frac{\delta I}{8h}\cdot\frac{l_{KTP}}{l_{opo}}\cdot E_p(r,t)E_s(r,t)E_i(r,t)\right]\cdot 2\pi r dr \tag{5}$$

$$\int_0^\infty \frac{d\phi_i(r,t)}{dt}\cdot 2\pi r dr = \int_0^\infty \left[-\frac{\phi_i(r,t)}{\tau_s} + \frac{\delta I}{8h}\cdot\frac{l_{KTP}}{l_{opo}}\cdot E_p(r,t)E_s(r,t)E_i(r,t)\right]\cdot 2\pi r dr \tag{6}$$

$$\int_0^\infty \frac{dn(r,t)}{dt}\cdot 2\pi r dr = \int_0^\infty \left[R_{in}e^{-\frac{2r^2}{w_p^2}} - \sigma c\phi_g(r,t)n(r,t) - \frac{n(r,t)}{\tau}\right]\cdot 2\pi r dr \tag{7}$$

$$\int_0^{r_y} \frac{dn_{y1}(r,t)}{dt}\cdot 2\pi r dr = \int_0^{r_y} \left[\frac{n_{y0} - n_{y1}(r,t)}{\tau_y} - \frac{\varepsilon_p}{4h\omega_p}\cdot\sigma_g c n_{y1}(r,t)E_p^2(r,t)\right]\cdot 2\pi r dr \tag{8}$$

Equation (4) describes the loss of fundamental-light photons by thermal effect, AO crystal and nonlinear transformation of the KTP crystal. In the equation, $-\left[(\sigma_g - \sigma_e) l_y n_{y1}(r,t)\phi_y(r,t) + \sigma_e l_y n_{y0}\phi_y(r,t)\right]$ represents the loss of fundamental-light photons by PtS_2 SA. The gain of signal-light and idler-light photons with time can be described by Equations (5) and (6). Equation (7) shows the loss of the population inversion in the laser medium. In the equations, t_r is the round-trip time of the fundamental light. l, l_g, l_{KTP} and l_{OPO} are the physical lengths of the laser cavity, the gain medium, KTP crystal, and OPO cavity. ε_j ($j = p, s, i$) is the dielectric constant and the frequency of the three lights. In Equation (4), δ_T is the diffractive loss caused by the gain medium's thermal effect. $\delta_a(t)$ can be written as [32],

$$\delta_a(t) = \delta_a\exp\left[-\left(\frac{t}{t_{AO}}\right)^2\right] \tag{9}$$

where t_{AO} and δ_a are the turn-off time and the intrinsic diffraction loss of the AO Q-switch. $\delta_a(t)$ is used to describe the loss function of the gradual AO modulator (AOM) caused by the exponential time delay. The basic parameters for calculating the rate equation refer to previous work [32–35].

3.2. PtS_2 SA Parameters Derivation by Inhomogeneously Broadening Mechanism

For PtS_2 SA, the change of the population inversion density is shown in Equation (8). σ_g and σ_e are the ground-state and excited-state absorption cross-sections of SA, which are

essential parameters to characterize saturable-absorption properties of SA. By using the information in reference [33], we can obtain the relationship between them.

$$\frac{\sigma_g}{\sigma_e} = \frac{\ln T_0}{\ln T_{\max}} \tag{10}$$

$$\frac{(\sigma_g - \sigma_e) \times T_0}{h\upsilon} = k \tag{11}$$

The values of small-signal transmittance (T_0) at a low power density, maximum transmittance ($T_{\max}$) at a high power density, and slope k were obtained, as shown in Figure 2. Then, the values of σ_g and σ_e for the 6.2 nm-thickness PtS_2 SA can be estimated to be 6.4298×10^{-19} cm^{-2} and 2.5927×10^{-19} cm^{-2}. Considering the inhomogeneously broadening mechanism, the excited-state lifetime of PtS_2 is calculated to be 1.043 ms [33]. Table 1 demonstrates the calculated key parameters of PtS_2 SA.

Table 1. The key parameters for saturable absorption properties of 2D-PtS_2 SA.

Parameters	Values
σ_g	6.4298×10^{-19} cm^{-2}
σ_e	2.5927×10^{-19} cm^{-2}
τ_y	1.043 ms
l_y	6.2 nm
n_{y0}	5.64×10^{24} cm^{-3}

These parameters can be substituted into Equations (4)–(8), which are solved by computer programming. In addition, Equations (4), (7), and (8) could dynamically model a PtS_2 SA passively Q-switched laser.

4. Optimized Experiment of Q-Switched IOPO Based on PtS_2 SA

4.1. Experimental Setup

The experimental setup for doubly Q-switched Nd^{3+}: YVO_4 IOPO with AO modulator (AOM) and PtS_2 SA is shown in Figure 3. A commercial LD with 400 μm beam diameter is used as the pump source, and the 808 nm-wavelength laser from LD is focused by the 1:0.5 coupled lens. The gain medium used in the experiment is a Nd:YVO_4 laser crystal with a $3 \times 3 \times 5$ mm^3 size and 0.6 at.% Nd^{3+} dope. The two faces of the crystal were antireflection (AR)-coated at both 808 nm and 1064 nm wavelengths. The $5 \times 5 \times 20$ mm^3 KTP crystal with type II non-critical phase-matching configuration ($\theta = 90°$, $\varphi = 0°$) along X-axis is applied to obtain a maximum effective nonlinear coefficient. The fundamental cavity length is about 125 mm, which is from mirror M_1 to M_2. The OPO cavity length is about 28 mm, and the signal light oscillates between M_2 and the first side of KTP. The repetitions of AO were 15 kHz and 25 kHz, respectively.

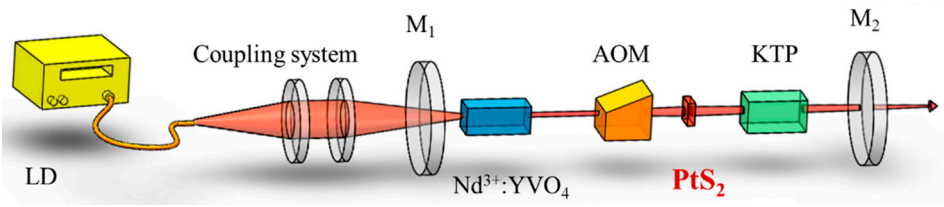

Figure 3. Experimental setup of the IOPO pumped by a doubly Q-switched Nd^{3+}: YVO_4 laser with AOM and PtS_2 SA.

A laser power meter (MAX500AD, Coherent Inc., Santa Clara, CA, USA) was employed to measure the laser average output power. Two fast photo-electronic diodes (with a rising time of 1 ns) and a digital oscilloscope (TDS620B, Tektronix, Beaverton, OR, USA) were used to measure the fundamental-pulse and the signal-pulse temporal characteristics of the

output, respectively. A spectrometer (MS9710C, Anritsu, Atsugi, Japan), working in the wavelength range of 600–1750 nm, was employed to record the laser spectrum.

4.2. Experimental Results and Discussion

The output spectrum of doubly Q-switched IOPO is shown in Figure 4a,b. The fundamental and signal light wavelengths are found to locate at 1064 nm and 1570 nm, respectively.

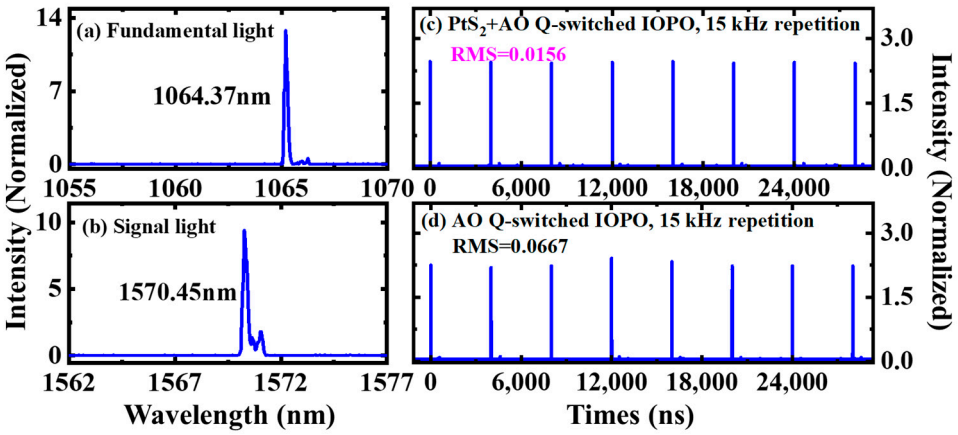

Figure 4. Spectrum and temporal pulse train. (**a**,**b**), corresponding spectrum from active–passive Q-switched IOPO at incident pump of 5.0 W and f_p = 15 kHz. (**c**,**d**), typical temporal pulse train of signal light from Q-switched IOPO, under incident pumped power of 5.2 W and f_p = 15 kHz. RMS: root means square error.

Figure 4c,d display the typical pulse trains of signal light from two kinds of IOPO, under the AOM repetition rate of 15 kHz and incident pumped power of 5.0 W. The root means square error (RMS) of peak-to-peak jitter for signal light output from the doubly Q-switched IOPO is only 0.0156 value was much smaller than the 0.0667 RMS of AO singly Q-switched IOPO. As shown in Figure 4, it was concluded that the application of PtS_2 SA effectively improves the peak-to-peak pulse stability of Q-switched IOPO.

The laser characteristics of AO active Q-switched IOPO and PtS_2 + AO dual-loss modulated Q-switched IOPO at two different AO modulation rates, as shown in Figure 5. Figure 5a,c show the average output powers of these two kinds of modulation versus the incident pump powers. The 1570 nm-wavelength average output power of the singly loss-modulated IOPO was indeed higher than the dual-loss-modulated IOPO. This is attributed to the insert loss of PtS_2 SA. Compared to 3.0 W threshold of AO Q-switched IOPO, the threshold pump power of the dual-loss Q-switched operation increased to 3.6 W.

The pulse width of signal light with different pulse repetitions is shown in Figure 5b,d, which commonly declines with increasing pump power but increases with a rising AO repetition rate. In a dual-loss Q-switched laser, the number of longitudinal modes could be suppressed by the participation of SA, and then the pulse width could be cut down. Therefore, in Figure 5b,d, the signal-light pulse from IOPO pumped by a PtS_2 + AO doubly Q-switched laser was shorter than that from IOPO pumped by AO singly Q-switched laser. Because of PtS_2's saturable absorption to fundamental laser, the signal-light pulse width is 64.3% compressed from 6.102 ns to 2.178 ns at 15 kHz pulse-repetition rate and 5.2 W pump power.

With the average output power and the repetition frequency of the pulse, the pulse energy of the signal light could be calculated by $E_{pulse} = P_{average}/f_p$, which is shown in Figure 5e,g. Then, the peak power was calculated by $P_{peak} = E_{pulse}/W$, where W is the full width at half maximum (FWHM) of the signal pulse [32], shown in Figure 5f,h. Owing to the pulse compression of PtS_2 SA, the peak power of dual-loss Q-switched IOPO increased 131% from 1.815 kW in single Q-switched IOPO to 4.193 kW in doubly Q-switched one at 5.2 W pump power.

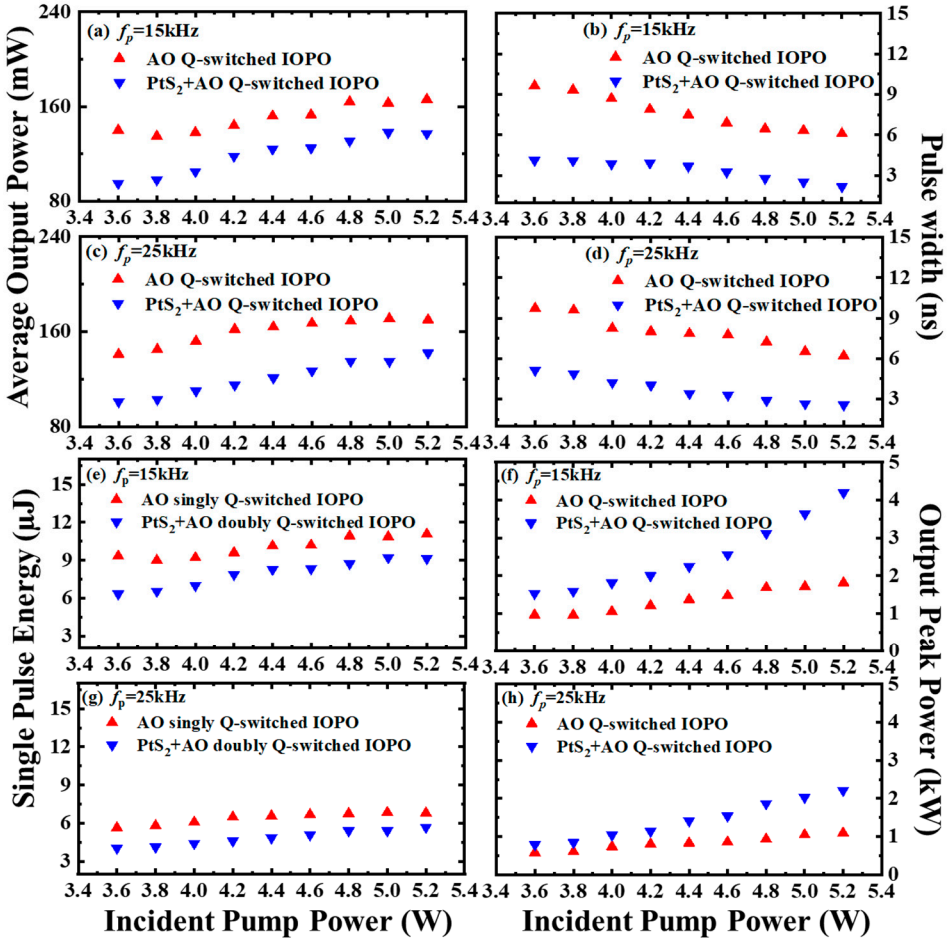

Figure 5. Output characteristics from two kinds of Q-switched IOPO. (**a**,**c**), average output power. (**b**,**d**), pulse width. (**e**,**g**), single pulse energy. (**f**,**h**), peak power.

The temporal pulse profiles of fundamental and signal waves are shown in Figure 6a–d for two IOPOs at the incident pump power of 5.2 W and AO modulation rate of 15 kHz. In Figure 6a, the 1064 nm fundamental-pulse profile leaking from IOPO is shown, and so is the undepleted 1064 nm pulse profile from the AO Q-switched laser without IOPO. For comparison, the depleted and undepleted 1064 nm-pulse temporal profiles from the PtS_2-based IOPO and laser are shown in Figure 6c. Because of PtS_2's saturable absorption, the consumption of fundamental-light energy is larger in doubly Q-switched IOPO than that in AO Q-switched IOPO. In Figure 6e, the fundamental-to-signal conversion efficiency is calculated with the consumption of 1064 nm laser demonstrated in Figure 6a,c. Under incident pump powers of 5.2 W and f_p = 15 kHz, the nonlinear conversion efficiency of doubly Q-switched IOPO is 39.9%, which increased 13.2% compared to IOPO without PtS_2. The energy conversion from 808 nm-pump laser to 1570 nm-signal light is up to 3.29%.

By numerically solving the above-derived rate Equations (4)–(8), the temporal pulse from IOPO or laser could be calculated with PtS_2's SA parameters in Table 1. Figure 7a,b show the theoretical and experimental pulse profiles of the fundamental light and signal light at 5.2 W pump power and 15 kHz AO-modulating rate. Figure 7c provides the calculated 1064 nm-wavelength pulse train of the PtS_2 singly Q-switched laser. It can be seen that the theoretical values from Gaussian rate equations fit the experimental data well.

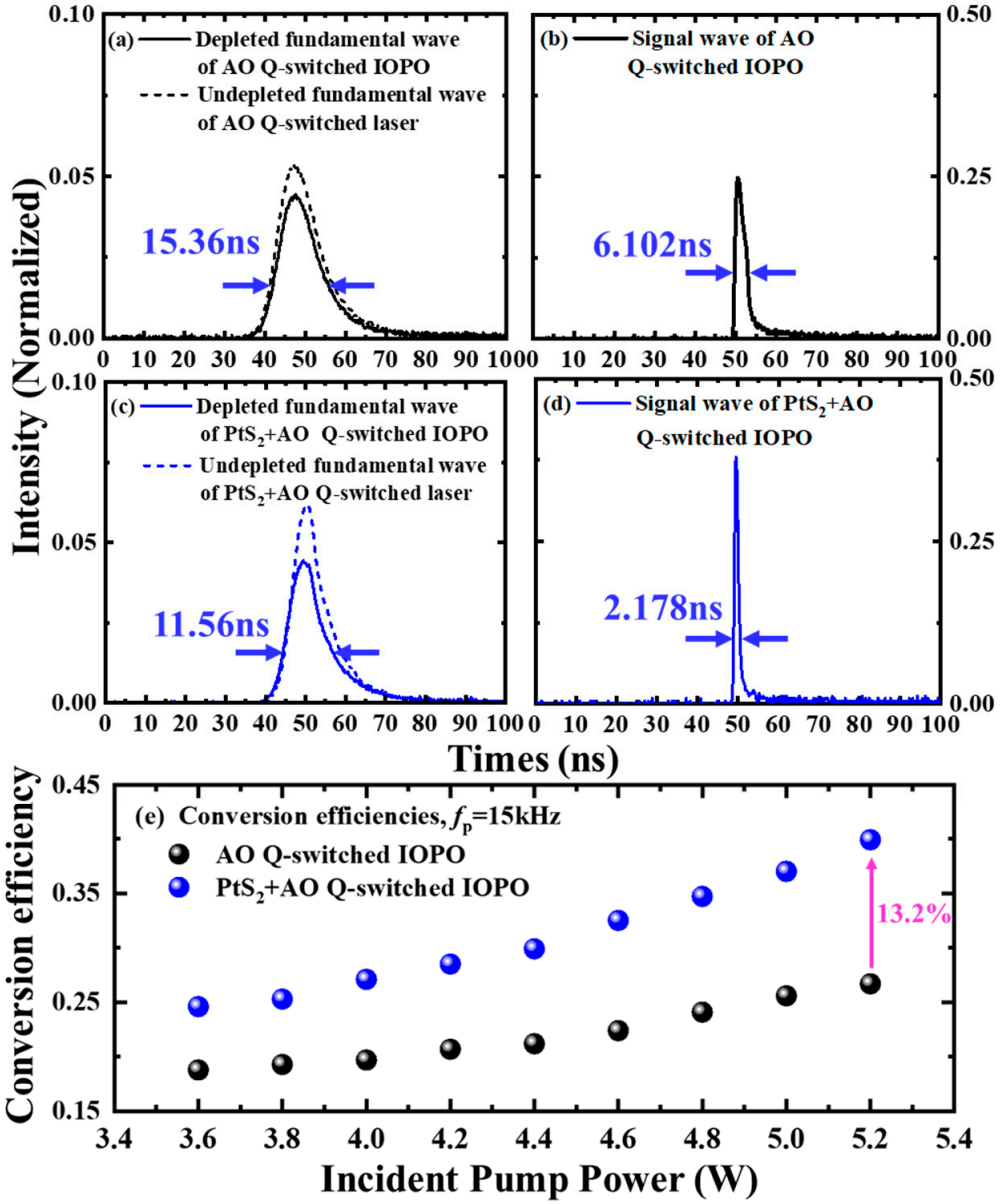

Figure 6. Investigation of IOPO's conversion efficiency. (**a**,**c**), undepleted and depleted fundamental-pulse profiles from Q-switched laser cavity under incident pumped power of 5.2 W and f_p = 15 kHz. (**b**,**d**), signal-pulse profiles from Q-switched IOPO under incident pump power of 5.2 W and f_p = 15 kHz. (**e**) fundamental-to-signal conversion efficiencies from two IOPOs versus incident pump power when f_p = 15 kHz.

Several SAs have been used to improve the performance of IOPO. In Table 2, the output characteristics of doubly Q-switched IOPO with AOM and different SA are reviewed. Compared to other SAs, the 6.2 nm-thickness PtS_2 used in this work could optimize IOPO's operation at lower incident pump power ($\leq$5.2 W). Meanwhile, doubly Q-switched IOPO based on PtS_2 attains 3.6 W, the lowest threshold, and 3.29%, the highest pump-to-signal conversion efficiency.

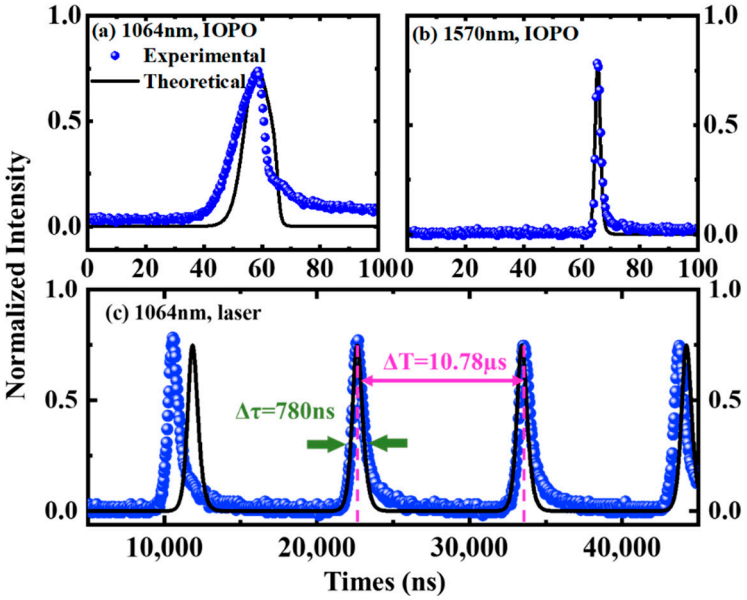

Figure 7. Theoretical fit of temporal-pulse profile output from Q-switched laser or IOPO based on PtS_2 SA. (**a**) Temporal-pulse profile of the fundamental light. (**b**) Temporal-pulse profile of the signal light. (**c**) Pulses from PtS_2 SA passively Q-switched laser. Solid, calculated values from rate equations. Scatter, experimental data.

Table 2. Performances of KTP-IOPOs pumped by doubly Q-switched lasers with an AOM and different SA.

Q-Switching Method	Nonlinear Medium	Max Pump Power (808 nm)	Threshold Value (1570 nm)	Peak Power (1570 nm)	Conversion Efficiency at Max Pump Power (808→1570 nm)	Ref
AOM + Cr^{4+}:YAG	KTP	6.3 W	5.1 W	2.25 kW	1.19%	[32]
AOM + monolayer graphene SA		11.7 W	5.2 W	7.9 kW	0.81%	[36]
AOM + MoS_2 SA		10.2 W	5.6 W	21.6 kW	1.79%	[37]
AOM + $MoSe_2$ SA		7.6 W	6.0 W	3.37 kW	1.46%	[33]
AOM + WS_2 SA		10.2 W	5.2 W	28.7 kW	2.28%	[38]
AOM + PtS_2 SA		5.2 W	3.6 W	4.193 kW	3.29%	This work

5. Conclusions

In conclusion, a 6.2 nm-thickness PtS_2 SA was prepared using the method of EBE combined with post-sulfurization. Based on the measured nonlinear transmittance, the ground-state and the excited-state absorption cross-sections of PtS_2 SA were estimated to be 6.4298×10^{-19} cm^{-2} and 2.5927×10^{-19} cm^{-2}, and the excited-state lifetime was approximately 1.043 ms. In the experiment, a KTP IOPO pumped by an active–passive Q-switched fundamental laser with AOM + PtS_2 was realized. With the application of PtS_2 SA, the peak-to-peak stability of Q-switched IOPO improved by 76.6%. The pulse width of signal light was 64.3% compressed, and the peak power improved 131%. In particular, due to PtS_2-SA's optimization, the conversion efficiency of IOPO improved by 13.2%. To the best of our knowledge, the 3.29% pump-to-signal conversion efficiency is the highest value to date for the doubly Q-switched IOPO with AOM. In theory, the rate equations under Gaussian assumption are derived and numerically solved with PtS_2's SA parameters. The theoretical values fit the experiment ones well.

Author Contributions: X.H. conceived and designed the experiments, performed the experiments and analyzed the data, drafted the manuscript; H.G. fabricated and characterized the PtS_2 saturable

absorber; J.W. and K.J. contributed to perform the theoretical analysis; W.T. and W.X. provided some experimental equipment, and all authors contributed to writing and editing the manuscript. All authors have read and agreed to the published version of the manuscript.

Funding: This work was supported by the Natural Science Foundation of Shandong Province, grant number ZR2021MF128; National Natural Science Foundation of China, grant numbers 62005049 and 61308057; Doctoral Fund Project from University of Jinan, grant number XBS1917.

Institutional Review Board Statement: Not applicable.

Informed Consent Statement: Not applicable.

Data Availability Statement: Not applicable.

Conflicts of Interest: The authors declare no conflict of interest.

References

1. Manzeli, S.; Ovchinnikov, D.; Pasquier, D.; Yazyev, O.V.; Kis, A. 2D transition metal dichalcogenides. *Nat. Rev. Mater.* **2017**, *2*, 1–15. [CrossRef]
2. Ren, K.; Zhu, Z.; Wang, K.; Huo, W.; Cui, Z. Stacking-Mediated Type-I/Type-II transition in two-dimensional $MoTe_2/PtS_2$ Heterostructure: A first-principles simulation. *Crystals* **2022**, *12*, 425. [CrossRef]
3. Muhsen Almayyali, A.O.; Kadhim, B.B.; Jappor, H.R. Tunable electronic and optical properties of 2D PtS_2/MoS_2 van der Waals heterostructure. *Physica E* **2020**, *118*, 113866. [CrossRef]
4. Yan, H.-J.; Li, Z.; Liu, S.-C.; Wang, X.; Zhang, X.; Xue, D.-J.; Hu, J.-S. Investigation of weak interlayer coupling in 2D layered GeS_2 from theory to experiment. *Nano Res.* **2021**, *15*, 1013–1019. [CrossRef]
5. Long, H.; Tang, C.Y.; Cheng, P.K.; Wang, X.Y.; Qarony, W.; Tsang, Y.H. Ultrafast laser pulses generation by using 2D layered PtS_2 as a saturable absorber. *J. Lightwave Technol.* **2019**, *37*, 1174–1179. [CrossRef]
6. Zhao, D.; Xie, S.; Wang, Y.; Zhu, H.; Chen, L.; Sun, Q.; Zhang, D.W. Synthesis of large-scale few-layer PtS_2 films by chemical vapor deposition. *AIP Adv.* **2019**, *9*, 025225. [CrossRef]
7. Liu, G.; Gan, Y.; Quhe, R.; Lu, P. Strain dependent electronic and optical properties of PtS_2 monolayer. *Chem. Phys. Lett.* **2018**, *709*, 65–70. [CrossRef]
8. Lu, J.; Zhang, X.; Su, G.; Yang, W.; Han, K.; Yu, X.; Wan, Y.; Wang, X.; Yang, P. Large-area uniform few-layer PtS_2: Synthesis, structure and physical properties. *Mater. Today Phys.* **2021**, *18*, 100376. [CrossRef]
9. Wang, X.; Long, H.; Qarony, W.; Tang, C.Y.; Yuan, H.; Tsang, Y.H. Fabrication of luminescent PtS_2 quantum dots. *J. Lumin.* **2019**, *211*, 227–232. [CrossRef]
10. Wang, X.; Cheng, P.K.; Tang, C.Y.; Long, H.; Yuan, H.; Zeng, L.; Ma, S.; Qarony, W.; Tsang, Y.H. Laser Q-switching with PtS_2 microflakes saturable absorber. *Opt. Express* **2018**, *26*, 13055–13060. [CrossRef]
11. Li, L.; Wang, W.; Chai, Y.; Li, H.; Tian, M.; Zhai, T. Few-Layered PtS_2 phototransistor on h-BN with high gain. *Adv. Funct. Mater.* **2017**, *27*, 1701011. [CrossRef]
12. Almayyali, A.O.M.; Kadhim, B.B.; Jappor, H.R. Stacking impact on the optical and electronic properties of two-dimensional $MoSe_2/PtS_2$ heterostructures formed by PtS_2 and $MoSe_2$ monolayers. *Chem. Phys.* **2020**, *532*, 1–7. [CrossRef]
13. Ma, P.; Lin, W.; Zhang, H.; Xu, S.; Yang, Z. High-Power large-energy rectangular mode-locked Er-Doped fiber laser based on high-damage-threshold MoS_2 saturable absorber. *IEEE Photonics J.* **2019**, *11*, 1–12. [CrossRef]
14. Zhao, Y.; Qiao, J.; Yu, P.; Hu, Z.; Lin, Z.; Lau, S.P.; Liu, Z.; Ji, W.; Chai, Y. Extraordinarily strong interlayer interaction in 2D layered PtS_2. *Adv. Mater.* **2016**, *28*, 2399–2407. [CrossRef] [PubMed]
15. Wang, Z.; Wang, P.; Wang, F.; Ye, J.; He, T.; Wu, F.; Peng, M.; Wu, P.; Chen, Y.; Zhong, F.; et al. A noble metal dichalcogenide for high-performance field-effect transistors and broadband photodetectors. *Adv. Funct. Mater.* **2019**, *30*, 1907945. [CrossRef]
16. Yu, Y.; Chen, X.; Cheng, L.; Li, S.; Wu, C.; Dong, Y.; Fu, Y.; Jin, G. Continuous-Wave intracavity multiple optical parametric oscillator using an aperiodically poled lithium niobate around 1.57 and 3.84 μm. *IEEE Photonics J.* **2017**, *9*, 1–8. [CrossRef]
17. Myers, L.E.; Bosenberg, W.R. Periodically poled lithium niobate and quasi-phase-matched optical parametric oscillators. *IEEE J. Quantum Electron.* **1997**, *33*, 1663–1672. [CrossRef]
18. Ding, Z.; Liu, P.; Li, Y.; Zhang, Z. Continuous-wave, singly-resonant, intracavity optical parametric oscillator based on a single-mode-laser-diode-pumped Yb:KYW laser. *Opt. Lett.* **2018**, *43*, 2807–2810. [CrossRef]
19. Debuisschert, T.; Raffy, J.; Pocholle, J.P.; Papuchon, M. Intracavity optical parametric oscillator: Study of the dynamics in pulsed regime. *J. Opt. Soc. Am. B* **1996**, *13*, 1569–1587. [CrossRef]
20. Zhang, H.; Zhao, S.; Zhao, J.; Yang, K.; Li, G.; Li, D.; Li, T.; Qiao, W.; Wang, Y. Generation of low repetition rate sub-nanosecond pulses in doubly QML Nd:Lu0.5Y0.5VO_4 and Nd:YVO_4 lasers with EO and transmission SSA. *Opt. Laser Technol.* **2015**, *69*, 39–43. [CrossRef]
21. Chen, L.; Li, X.; Zhang, H.; Xia, W. Passively Q-switched 1.989μm all-solid-state laser based on a WTe_2 saturable absorber. *Appl. Opt.* **2018**, *57*, 10239–10242. [CrossRef] [PubMed]

22. Tian, K.; Li, Y.; Yang, J.; Dou, X.; Xu, H.; Han, W.; Liu, J. Passively Q-switched Yb:KLu(WO_4)$_2$ laser with 2D $MoTe_2$ acting as saturable absorber. *Appl. Phys. B* **2019**, *125*, 1–6. [CrossRef]
23. Liu, F.Q.; Xia, H.R.; Pan, S.D.; Gao, W.L.; Ran, D.G.; Sun, S.Q.; Ling, Z.C.; Zhang, H.J.; Zhao, S.R.; Wang, J.Y. Passively Q-switched Nd:$LuVO_4$ laser using Cr^{4+}:YAG as saturable absorber. *Opt. Laser Technol.* **2007**, *39*, 1449–1453. [CrossRef]
24. Wagner, W.G.; Lengyel, B.A. Evolution of the giant pulse in a laser. *J. Appl. Phys.* **1963**, *34*, 2040–2046. [CrossRef]
25. Oshman, M.; Harris, S. Theory of optical parametric oscillation internal to the laser cavity. *IEEE J. Quantum Electron.* **1968**, *5*, 491–502. [CrossRef]
26. Li, G.; Zhao, S.; Yang, K.; Wu, W. Pulse width reduction in diode-pumped Nd:$GdVO_4$ laser with AO and GaAs double Q-switches. *Jpn. J. Appl. Phys.* **2005**, *44*, 3017–3021. [CrossRef]
27. Yang, K.; Zhao, S.; Li, G.; Zhao, H. Compression of pulse duration in a laser-diode, end-pumped, double Q-switched laser. *Appl. Opt.* **2005**, *44*, 271–277. [CrossRef]
28. Deng, Y.; Liu, Z.; Wang, A.; Sun, D.; Chen, Y.; Yang, L.; Pang, J.; Li, H.; Zhou, W. Oxygen-incorporated MoX (X: S, Se or P) nanosheets via universal and controlled electrochemical anodic activation for enhanced hydrogen evolution activity. *Nano Energy* **2019**, *62*, 338–347. [CrossRef]
29. Kjekshus, A.; Grnvold, F.; Jrgensen, P.M.; Refn, S. High Temperature X-Ray Study of the Thermal Expansion of PtS_2, $PtSe_2$, $PtTe_2$ and $PdTe_2$. *Acta Chem. Scand.* **1959**, *13*, 1767–1774. [CrossRef]
30. Miro, P.; Ghorbani-Asl, M.; Heine, T. Two dimensional materials beyond MoS_2: Noble-transition-metal dichalcogenides. *Angew. Chem. Int. Ed. Engl.* **2014**, *53*, 3015–3018. [CrossRef]
31. Wang, K.; Yang, K.; Zhang, X.; Zhao, S.; Luan, C.; Liu, C.; Wang, J.; Xu, X.; Xu, J. Passively Q-Switched Laser at 1.3 μm With Few-Layered MoS_2 Saturable Absorber. *IEEE J. Sel. Top. Quantum Electron.* **2017**, *23*, 71–75. [CrossRef]
32. Wang, J.; Zhao, S.; Li, G.; Yang, K.; Li, D.; An, J.; Li, M. Pulse Compression in Laser-Diode-Pumped Doubly Q-Switched intracavity optical parametric oscillator considering gaussian distribution of intracavity photon densities. *Jpn. J. Appl. Phys.* **2007**, *46*, 1505–1510. [CrossRef]
33. Wang, J.; Pang, J.B.; Liu, S.P.; Zhang, H.K.; Tang, W.J.; Xia, W. Experimental and dynamical study of a dual Q-switched intracavity OPO based on few-layer $MoSe_2$ SA. *Opt. Express* **2019**, *27*, 36474–36486. [CrossRef] [PubMed]
34. Friel, G.J.; Conroy, R.S.; Kemp, A.J.; Sinclair, B.D.; Ley, J.M. Q-switching of a diode-pumped Nd:YVO4 laser using a quadrupole electro-optic deflector. *Appl. Phys. B* **1998**, *67*, 267–270. [CrossRef]
35. Wang, J.; Zhao, S.; Yang, K.; Dong, L.; Li, G.; Li, D.; Li, M.; An, J.; Qiao, W. Pulse compression and threshold decrease in highrepetition-rate doubly Q-switched intracavity optical parametric oscillator. *J. Opt. Soc. Am. B* **2007**, *24*, 2521–2525. [CrossRef]
36. Qiao, J.P.; Zhao, J.; Yang, K.J.; Zhao, S.Z.; Li, G.Q.; Li, D.C.; Li, T.; Qiao, W.C.; Chu, H. Intracavity KTP OPO pumped by a doubly Q-switched laser with AOM and a monolayer graphene saturable abosorber. *Opt. Mater.* **2015**, *50*, 234–237. [CrossRef]
37. Qiao, J.P.; Zhao, S.Z.; Yang, K.J.; Zhao, J.; Li, G.Q.; Li, D.C.; Li, T.; Qiao, W.C. Hybrid Q-switched laser with MoS_2 saturable absorber and AOM driven sub-nanosecond KTP-OPO. *Opt. Express* **2017**, *25*, 4227–4238. [CrossRef]
38. Qiao, J.P.; Zhao, S.Z.; Yang, K.J.; Zhao, J.; Li, G.Q.; Li, D.C.; Li, T.; Qiao, W.C.; Wang, Y.G. Sub-nanosecond KTP-OPO pumped by a hybrid Q-switched laser with WS_2 saturable absorber and AOM. *Opt. Mater. Express* **2017**, *7*, 3998–4009. [CrossRef]